ADVANCED MATERIALS TECHNOLOGIES
www.advmattechnol.de

Water Transfer Printing Enhanced by Water-Induced Pattern Expansion: Toward Large-Area 3D Electronics

Brice Le Borgne, Siyi Liu, Xavier Morvan, Samuel Crand, Radu Alexandru Sporea, Nanshu Lu, and Maxime Harnois**

Perfectly wrapping planar electronics to complex 3D surfaces represents a major challenge in the manufacture of conformable electronics. Intuitively, thinner electronics are easier to conform to curved surfaces but they usually require a supporting substrate for handling. The water transfer printing (WTP) technology utilizes water surface tension to keep ultrathin electronics floating flat without supporting substrate, enabling their conformal transfer on 3D surfaces through a dipping process. In many cases, however, the size of the microfabricated electronics is much smaller than the target 3D surface. This work proposes that such mismatch in size can be overcome by leveraging stretchable electronics in WTP. Stretchable electronics are compliant to in-plane stretch induced by water surface tension, hence can first self-expand in water and then be transferred onto 3D objects. Uniaxial and biaxial expansion ranging from 41% to 166% has been achieved without any externally applied tension. The results demonstrate that expansion-enhanced WTP is a promising fabrication process for conformable electronics on large 3D surfaces.

1. Introduction

Currently, integrated circuits and microelectromechanical systems (MEMS) have to be fabricated on rigid planar wafers that cannot fit the shape of a 3D object. Emerging flexible and stretchable electronics offer a possible remedy for electronics conformable to 3D surfaces.[1–4] In the past few years, flexible and stretchable electronics have demonstrated many possibilities, including wearable and epidermal electronics,[5–11] implantable neuro monitors and stimulators,[12–14] soft optoelectronic devices,[15,16] deformable displays,[17–19] as well as conformal photovoltaic devices.[20] On the one hand, ultrathin flexible electronics have demonstrated extreme bendability.[21,22] Even so, wrinkles and folds are inevitable when wrapping flexible sheets on 3D surfaces with two nonzero principal curvatures. A recently developed curved image array demonstrated that selectively cutting the flexible sheet can effectively reduce folding and wrinkling when conforming it to a 3D surface.[23] On the other hand, stretchable electronics enabled by stretchable serpentine interconnects,[24,25] liquid metal,[26] nanomeshes[27] and nanoscrolls,[28] or intrinsically stretchable conductive and semiconducting polymers[29–32] are able to not only bend but also expand in-plane, hence capable of conforming to 3D surfaces such as spherical domes. But so far, there are limited studies on the conforming process, especially when the target object has a complex 3D surface. Except for conforming planar electronics to 3D surfaces, direct printing of electrical components on 3D surfaces has been demonstrated.[33] However, only limited materials such as conductive inks and devices such as 3D antenna can be printed so far. As a result, simple but versatile transferring techniques are in need for conformable electronics.

Water transfer printing (WTP) technology, also known as hydrographic printing, is commonly used to transfer planar graphics to 3D surfaces.[34] The process begins by printing graphics on a water-soluble substrate, which is then placed on water surface. As the substrate gets dissolved by water, the ultrathin graphics layer stays floating on water. A solid

Dr. B. Le Borgne, Dr. R. A. Sporea
Department of Electrical and Electronic Engineering
Advanced Technology Institute
University of Surrey
Guildford GU2 7XH, UK

S. Liu, Dr. N. Lu
Center for Mechanics of Solids, Structures and Materials
Department of Aerospace Engineering and Engineering Mechanics
The University of Texas at Austin
Austin, TX 78712, USA
E-mail: nanshulu@utexas.edu

The ORCID identification number(s) for the author(s) of this article can be found under https://doi.org/10.1002/admt.201800600.

DOI: 10.1002/admt.201800600

X. Morvan, Dr. S. Crand, Dr. M. Harnois
Département Microélectronique & Microcapteurs
Institut d'Électronique et des Télécommunications de Rennes
UMR CNRS 6164
Université Rennes 1
Campus de Beaulieu, 35042 Rennes Cedex, France
E-mail: maxime.harnois@univ-rennes1.fr

Dr. N. Lu
Department of Biomedical Engineering
Texas Materials Institute
The University of Texas at Austin
Austin, TX 78712, USA

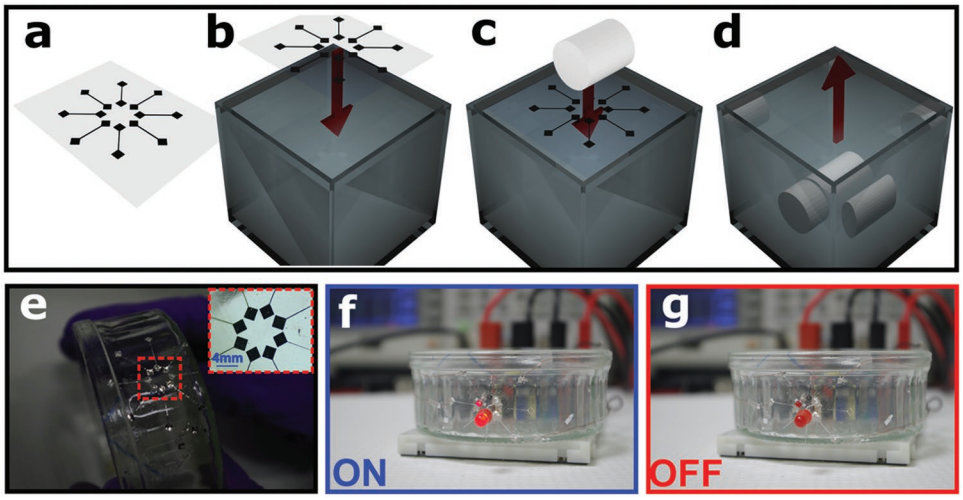

Figure 1. The WTP technology: sketches (a–d) illustrate the WTP process and images (e–g) demonstrate the aluminum interconnects are fully functional after transferred to a curved surface. a) Thin film aluminum patterned on PVA substrate; b) Float PVA on water held by a dip tank. c) After PVA dissolves, a 3D object dipped into the tank through the pattern. d) The 3D object is gently shaken in the water and then withdrawn from the water. e) Aluminum interconnects transferred onto a glass beaker, the inset highlights that interconnects do not contact each other. Optical images f) and g) demonstrate that a light emitting diode connected to power supply through the aluminum interconnects can be turned ON and OFF, respectively.

object is then slowly dipped into water through the floating graphics such that the graphics can wrap over and adhere by van der Waals force to the object surface, resulting in conformable graphical patterns on the 3D surface of the solid object. Recently, the field of conformable electronics has been inspired by the WTP.[35–37] Instead of printed graphics, ultrathin functional films and devices such as conductive interconnects, passive devices (i.e., metal/insulator/metal capacitors), and capacitive touchpads can be patterned on water-soluble substrates. When placed on water surface, the substrate dissolves, leaving only the functional layers floating on water. Dipping a solid object of complex 3D surface such as a model car or a donut-shaped object through the floating films results in high-conformability transfer on to very complex 3D surfaces.[35,38] Even though no expensive facility is required and the process is easy to implement, such degree of conformability on such complex 3D surfaces has never been achieved before. Furthermore, this process is applicable to different types of materials as long as they are thin enough. Proper patterning can further help eliminate wrinkles and folds after the transfer. Therefore, we believe that WTP holds great promise for the manufacture of future 3D conformable electronics.

Building upon the previous success, this work tries to apply WTP to cover large 3D surfaces by leveraging the expandability of stretchable electronics. Polyvinyl(alcohol) (PVA) is a well-known water-soluble polymer that has already been widely used in conventional WTP.[34] We will demonstrate that the pre-fabricated stretchable pattern on PVA substrate can significantly expand while PVA swells and dissolves in water, which does not require any external force and hence can be referred as *water-induced pattern expansion*. The expanded circuit can be transferred to a 3D surface much larger than the original size of the circuit. By combining the advantages of stretchable electronics and the WTP techniques, this new process allows the transfer of microfabricated wafer-scale electronics on much larger 3D objects.

This article is organized as follows. The WTP process will be described in Section 2.1 and the mechanism for water-induced pattern expansion will be explained in Section 2.2. Section 2.3 will discuss the control of this process such as pattern immobilization and controlled uniaxial expansion. As a demonstration, we patterned serpentine-shaped interconnects which expanded by 41% uniaxially before transferred onto a curvilinear object without any mechanical failure. Conclusions are offered in Section 3 and experimental details are available in Section 4.

2. Results and Discussion

2.1. Water Transfer Printing (WTP) Technology

The WTP process begins by fabricating ultrathin functional films on PVA. The materials and patterning methods can be applied as necessary, e.g., lithography for small-area processing with high-resolution or printed electronics for large-area patterning with mediocre resolution.[35] The details of the materials and patterning method in this study are described in Section 4. **Figure 1** shows that 150 nm thick aluminum was patterned via a shadow mask into an example radiating pattern with eight 15 mm long and 150 μm wide "rays" each terminated by two 2 mm × 2 mm squares on the PVA substrate (Figure 1a). After gently placing the specimen on water (Figure 1b), the PVA dissolved and the planar metal pattern floated on the water surface. A 3D object was slowly dipped into the water through the floating pattern such that as soon as the object contacts the pattern, the water applies a resistance to the dip which helps conform the pattern to object surface (Figure 1c). Upon full immersion, the whole planar pattern was transferred to the object. The pattern-covered object was gently shaken in the water and finally extracted out of the water (Figure 1d). The whole WTP process is shown in Video S1 in the Supporting

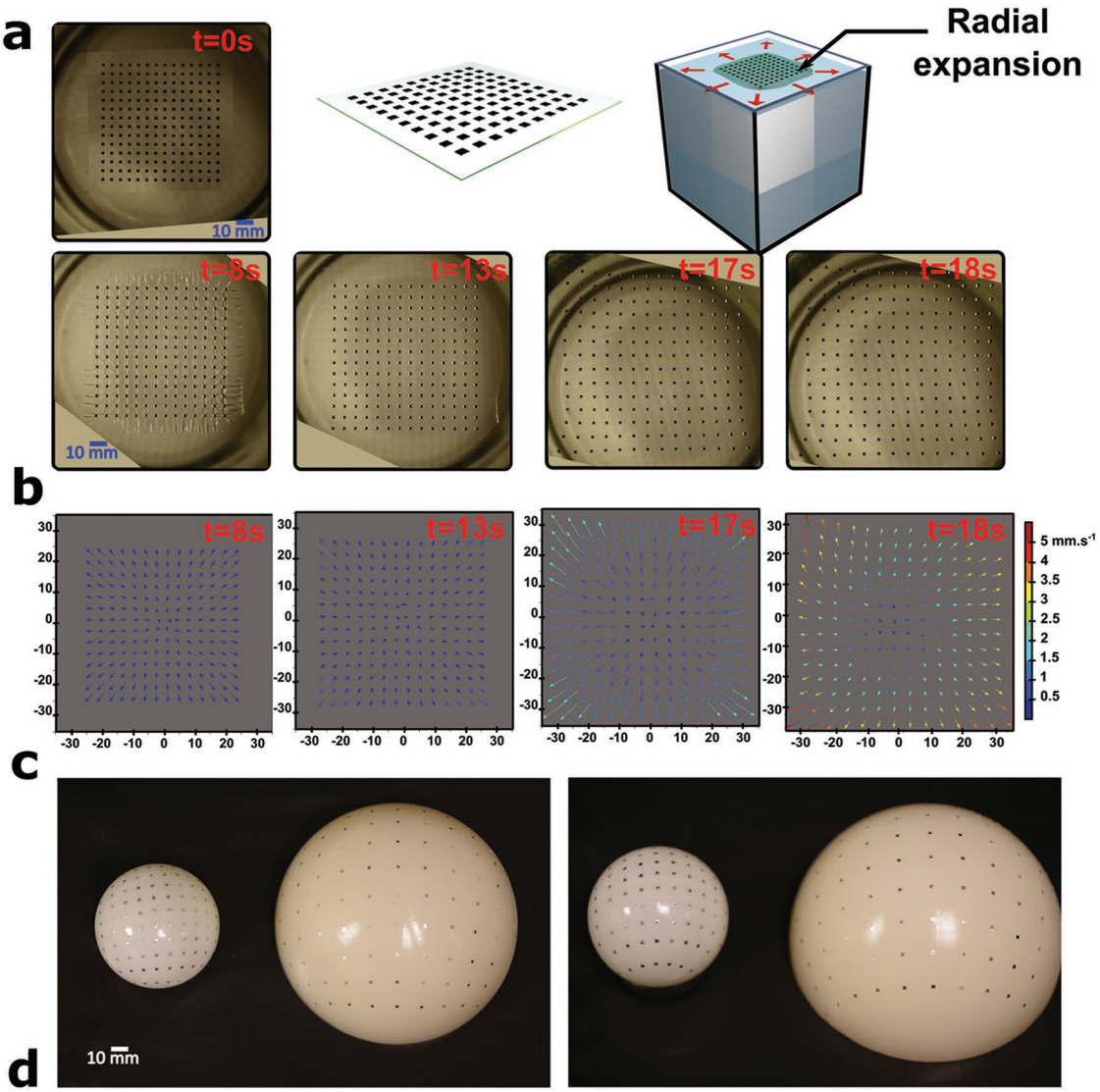

Figure 2. a) A schematic of an array of square-shaped aluminum islands patterned on a PVA substrate. When floating on water, the island array would undergo radial expansion. b) Snapshots of the square array on PVA on water showing that as PVA dissolves, the array expands. c) Displacement and velocity of each island after processing the images in (b). The length of each vector represents the displacement and the color of each vector color denotes the velocity. d) Images of the island array transferred on a table tennis ball (diameter 38 mm) before pattern expansion and on a hemispherical surface (diameter 80 mm) after pattern expansion. The left and right images show the top and a 45° tilted views, respectively.

Information. Figure 1e shows the radiating aluminum pattern transferred onto the sidewall of a glass beaker. After the transfer, the square terminals of the rays remained separated from each other, as shown in the inset of Figure 1e. Figure 1d,f highlights that surface-mounted devices such as light emitting diodes can be soldered to the aluminum terminals and be turned on afterwards, which verified the conductivity of these ribbons after WTP (see Figure S2 and Video S2 in the Supporting Information). In the current example pattern, the linear rays are not stretchable, and hence the transferred pattern well preserved the original design. If the pattern, however, is deformable in-plane, the PVA dissolution process may distort the pattern. Therefore, to achieve controlled pattern distortion, we first need to develop some basic understanding regarding the PVA dissolution process.

2.2. PVA Dissolution–Induced Pattern Expansion

When submerged in water, the mechanism of PVA dissolution has been investigated experimentally.[39] When PVA film is attacked by surrounding water from all directions, swelling and dissolution start simultaneously, but swelling can be observed much easier than dissolution because PVA is transparent. However, there is not yet available study on PVA dissolution when floating on water surface. The behavior would be different because water surface tension will come into play.

As PVA is transparent, to visualize PVA swelling and dissolution when floating on water surface, an array of 14 × 14 square-shaped aluminum islands (1 mm × 1 mm × 150 nm each with 3 mm distance) has been patterned on a PVA film as markers via a shadow mask (**Figure 2**a). It is reasonable to

assume that the thermally evaporated aluminum islands are perfectly bonded with the PVA film. Upon placing this PVA film on water surface, a gradual in-plane dilation of the square array can be observed, as shown in Figure 2b and Video S3 in the Supporting Information. The corresponding vector maps of the displacement (arrow length) and velocity (arrow color) of each island are displayed in Figure 2c. Combining Figure 2b and 2c, we conclude that the PVA dissolves through the following three-stage process. From 0 to 8 s (t = 0 s represents the moment that the device was placed on water), in Stage I, the PVA film swelled due to water uptake. Wrinkles formed perpendicular to the edges of the islands because of the compressive strain generated between the freely swelled PVA film and the unswelled part constrained by the stiff islands. From 8 to 17 s, in Stage II, PVA started obvious dissolving and hence softened to a point that it can be stretched by the surface tension of water at the edges of the film. As the expansion in Stage II is significant and controllable, we introduced a physical model to explain the mechanism in Notes S2 and S3 in the Supporting Information. After 17 s, in Stage III, the PVA film was fully dissolved in water and formed PVA/water mixture, which has lower surface tension than water.[40] Since the diffusion of PVA mixture took time, the PVA concentration was not uniform at liquid surface. The region of low PVA concentration close to the sidewall of the container would pull the Al islands away from the center of the container, where PVA concentration is high. It would drive the islands to further spread apart, initially at a faster speed than Stage II. As diffusion went on, the PVA concentration eventually became uniform in the tank, such that the surface tension gradient would eventually disappear. At this moment, there would be no more driving force for the island array to expand, so the island motion would eventually stop after the system reached new equilibrium. Note that if the pattern reaches the sidewall of the container, the pattern expansion would terminate before reaching equilibrium.

Optical images in Figure 2d illustrate the capability to achieve different transferred patterns in the WTP process from the same initial pattern. Two identical island arrays on PVA were transferred onto two distinct surfaces: a table tennis ball (38 mm in diameter) and a nylon hemisphere (80 mm in diameter). For the nylon hemisphere, a large tank was used in the experiments to allow the expansion of the PVA film. Although using the same initial pattern, the table tennis ball was dipped into water at t = 13 s, before the island array started to expand whereas the nylon hemisphere was dipped at t = 27 s, after the pattern fully expanded. For the pattern transferred on the hemisphere, the space between each square was designed to be 3 mm initially but became 8 mm ± 0.5 mm, corresponding to an increase of 166% ± 10%, after the WTP.

This experiment clearly demonstrates that a soft pattern on PVA can expand as PVA swells and dissolves on the water surface. Thus, it can enable the transfer of small-scale electronics to cover much larger 3D curvilinear surfaces. However, the expansion velocity is not constant during PVA dissolution and the stretching ratio of the film is not a linear function of time. Our experiment reveals that the expansion velocity first increases and then decreases with time until the expansion fully stops. Therefore, future research is required to quantitatively predict the pattern expansion process.

2.3. Pattern Control

2.3.1. Pattern Immobilization

As discussed in the previous section, PVA-dissolution-induced pattern expansion would distort the original design as time goes. It therefore requires a precise control of time in water if one hopes to transfer soft patterns with original design. If the time is too short, PVA is not fully dissolved. If the time is too long, the pattern gets distorted. And often there is no clear cut between the two. To preserve the original design during PVA dissolution, in our previous study, we added a thin stiff layer with mesh design on top of the actual pattern (Figure S4, Supporting Information). In this case, the expansion of the pattern can be suppressed but folds and wrinkles would form in the stiff layer if the target surface has sharp edges and complex geometry (see Figure S5 in the Supporting Information). Therefore, we want to propose a new idea for pattern immobilization here.

Figure 3a–c and Video S4 in the Supporting Information illustrate WTP under confinement. The 3D schematic in Figure 3a shows that the PVA-supported aluminum islands were placed on water surface with pre-installed rigid guides. The rigid guides were partly immersed in the water and kept stationary during the whole process to suppress pattern expansion during PVA dissolution.

Figure 3b offers the top view of the island array taken at t = 0, 20, and 80 s after it was placed on water surface. These snapshots indicate that the island array was fully confined by the rigid guides during the whole process. The vector maps of the displacement (Figure 3c) confirm that compared with the WTP experiments without rigid guides (Figure 2a), the pattern was immobilized by pre-installed rigid guides. It signifies that rigid guides can inhibit pattern expansion while still allowing PVA to dissolve. Thus, the aluminum island array in original design can be well preserved and transferred to a small object such as the table tennis ball without carefully controlling the time in water (see Figure S3 in the Supporting Information).

2.3.2. Controlled Anisotropic Pattern Expansion

Between free expansion and full immobilization, anisotropic expansion can also be achieved by installing a pair of fixed guides and a pair of mobile guides perpendicular to the fixed ones. The 3D schematic in **Figure 4**a and Video S5 in the Supporting Information illustrate the experimental setup for the WTP with anisotropic pattern expansion. At first, the PVA substrate was confined within a square zone defined by the fixed and the mobile guides perpendicular to the y and x axis, respectively. The mobile guides were free to move in the x direction. The materials and fabrication methods of the mobile guides is described in Experimental Section.

The top-view snapshots (Figure 4b) display the island pattern from 0 to 70 s. It is clear that the island pattern preferentially expanded along the x axis. Figure 4c plots the absolute island spacing (left axis) and the relative expansion (right axis) along the x direction (blue) and the y direction (red) as functions of time. Before 30 s, negligible stretching can be observed

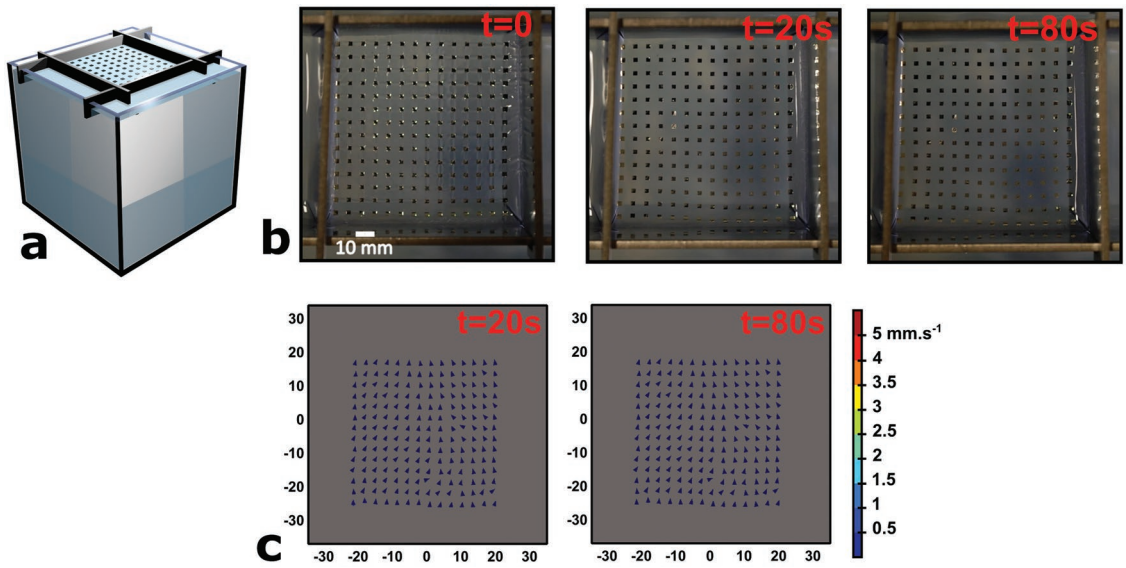

Figure 3. Pattern immobilization when confined by rigid guides. a) A 3D schematic of the specimen floating on water confined by quadrilateral rigid guides. b) Top-down snapshots for the island pattern at 0, 20, and 80 s. c) Displacement and velocity of each island at 20 and 80 s. The vector length and the color scale denote displacement and velocity, respectively.

in both directions. After 46 s, expansion in the x direction dominated and can be approximated to be uniaxial expansion. According to the plot in Figure 4c, expansion in the x direction grew exponentially with time whereas there was almost no motion in y axis after 46 s. Moreover, the standard deviations of the column/row spacing along both directions are negligible (<0.1 mm) compared with the average spacing (>2 mm) before 66 s. It signifies that the columns stayed as columns and the stretching was uniform before 66 s. The misalignment of the islands started to appear after 66 s, which indicates the loss of controlled uniaxial expansion, as denoted by the shaded zone in Figure 4c. A physical model is introduced to explain the mechanism of stretching in Notes S2 and S3 in the Supporting Information. The fitted solution is plotted in Figure 4c. As a result, we claim that this technique allows the pattern to undergo uniform uniaxial expansion up to 200%, allowing the transfer of large-scale 3D electronics using a small PVA substrate.

One demonstration for the WTP with anisotropic expansion is offered in Figure 4d,e. Two identical island patterns, one fully immobilized and one uniaxially expanded, were transferred onto two half cylinders of two different diameters, 40 and 80 mm in Figure 4d and 4e, respectively. One of the two patterns uniaxially expanded by 80% before transferred to the larger half cylinder. The side view of the half cylinders in Figure 4d,e highlights that pattern can be transferred on the curved 3D object without folds or losing alignment.

In addition to the island pattern, we also tested a ribbon pattern as shown in **Figure 5**. Twelve equally spaced straight aluminum ribbons (150 nm thick, 2 mm wide, and 45 mm long) were first fabricated on a PVA substrate. Rigid and mobile guides were placed perpendicular and parallel to the ribbons, respectively. Figure 5a shows the lateral expansion of the ribbons as the PVA film dissolved. The average misalignment angle after 52, 63, and 67 s are 0.7° ± 0.7°, 2° ± 1.5°, and 5.5° ± 3.5°, respectively. Only slight misalignment can be observed up to t = 63 s, when the pattern expanded 75% in the direction perpendicular to the linear ribbons. The expanded ribbon pattern was successfully transferred on a half cylinder (80 mm in diameter) at 60 s (Figure 5b). The expansion appeared to be 80% after the transfer, slightly more than 75%, which can be attributed to dipping-induced additional pattern expansion.

To add interconnects between the ribbons without adding too much mechanical resistance to lateral expansion, we propose to use a well-known soft and stretchable planar structure—the serpentine ribbons.[41,42] A 3D schematic for this experimental setup is provided in **Figure 6**a, where serpentine ribbons were aligned with the expansion direction as allowed by the mobile guides. Figure 6b and Video S6 in the Supporting Information show the water-induce separation of two parallel straight ribbons interconnected by serpentine ribbons. Figure 6c offers two images (front and back side) of the pattern after transferring on a hemicylindrical surface (50 mm in diameter). Compared with the original design, 41% uniaxial elongation was achieved without mechanical failure in the serpentine ribbons (Figure 6d), which was confirmed by the unchanged ohmic behavior between the straight ribbons before and after the WTP. Finite element analysis (FEA) was performed to estimate the local strain experienced by the serpentine ribbon after expansion (Figure S6 and Video S7 in the Supporting Information). Under 41% end-to-end tensile strain, the maximum principal strain in aluminum was found to be 2.52%, which is lower than the fracture strain of aluminum film of 150 nm thickness (2.68%).[43]

3. Conclusion

Our previous work has demonstrated that the WTP technology borrowed from hydrographics is capable of wrapping complex 3D surfaces with ultrathin flexible electronics. The

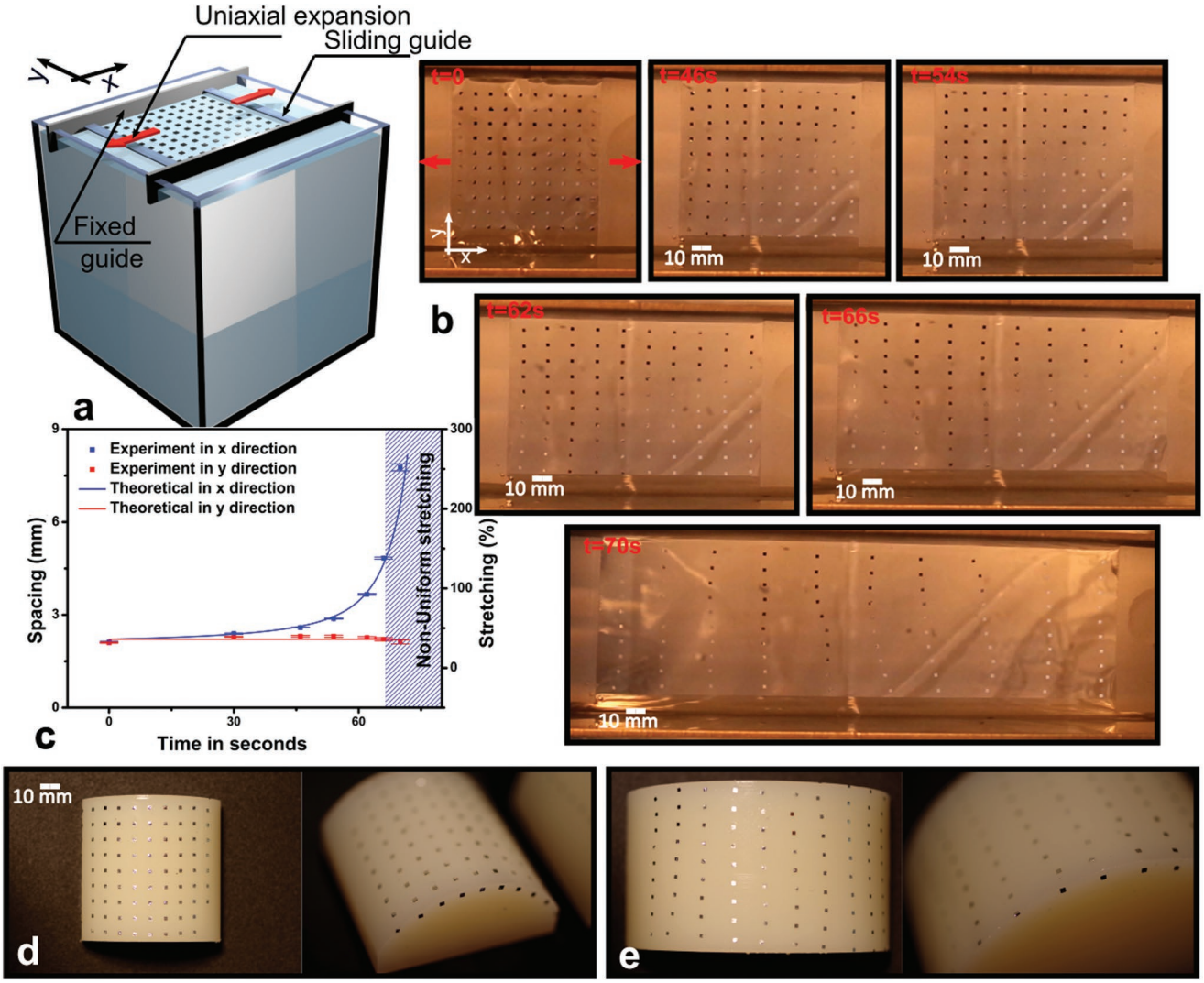

Figure 4. Uniaxial stretch–enhanced WTP. a) A 3D schematic showing the specimen confined by bilateral fixed guides which inhibit *y*-direction expansion and bilateral mobile guides which allow *x*-direction self-expansion. b) Six snapshots for the island pattern in water from 0 to 70 s. c) The pattern spacing and relative expansion in *x* (blue) and *y* (red) direction of experimental data (dot with error bar) and fitted solution (curve) plotted as functions of time. d) The immobilized pattern transferred to a small hemicylinder (40 mm diameter). e) The uniaxially expanded pattern transferred to a large hemicylinder (80 mm diameter).

compatibility with large-area electronics was thus proved as hand-sized objects were successfully comformally wrapped. In this work, we discovered that the dissolution of the PVA substrate induces omnidirectional self-expansion up to 166% in an island pattern if there is no external confinement. To achieve controlled pattern expansion, we found that installing fixed and mobile rigid guides on water surface was a simple and effective method. With the rigid guides, uniaxially expanded island and ribbon patterns were successfully achieved and transferred to hemicylindrical surfaces. Through the incorporation of stretchable structures such as serpentines, electrically conductive pathways can be preserved after the expansion and transfer without mechanical failure. During this process, water plays three different but essential roles: floating, expanding, and pressing the device pattern. We advocate that this expansion-enhanced WTP technique would improve and pave the way to new fabrication routes of large-area 3D conformable electronics using conventional wafer-based small-area microelectronics fabrication processes.

4. Experimental Section

Characterization: Top-view images and videos were obtained by PENTAX K70D equipped with a ZOOM macro 50 mm (Pentax). Electrical measurements were performed by using a probe station Keithley 2636A and Labview. Surface-mounted devices were connected to the aluminum terminals by conductive epoxy (reference CW2400; Chemtronics).

PVA Processing: First, photoresist was deposited on glass slide as a sacrificed layer to release the PVA substrate at the end of fabrication process. Then, a PVA solution (PVA; Mw 9000–10 000, 80% hydrolyzed from Aldrich) was prepared by mixing DI water and PVA powder

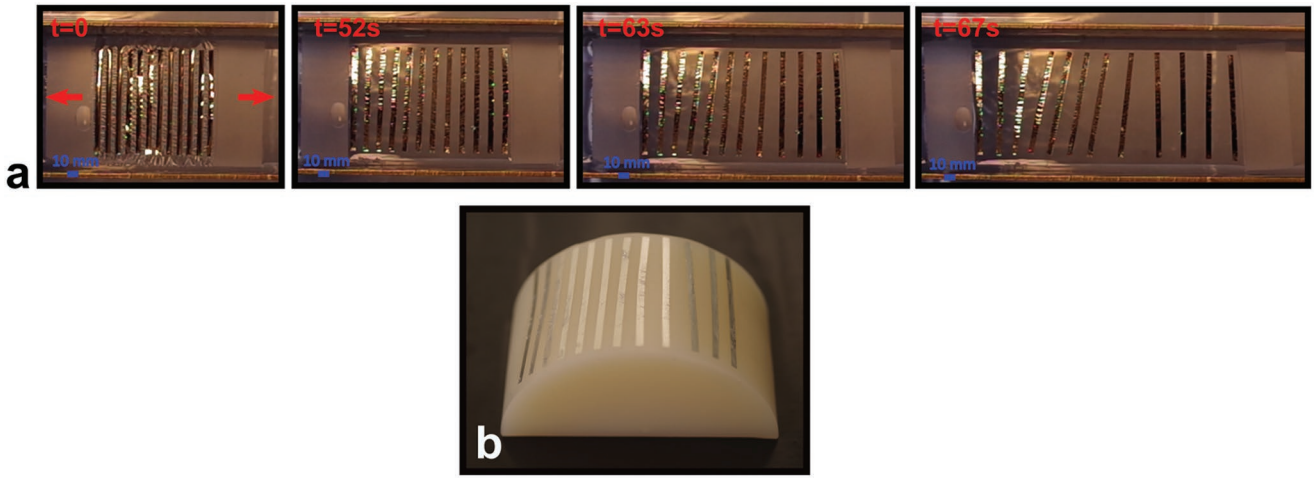

Figure 5. a) Snapshots of aluminum ribbon pattern uniaxially expanded from 0 to 67 s. b) The expanded ribbon pattern transferred onto a hemicylindrical surface of 80 mm diameter.

(5:1 w/w water/PVA) and filtering it with a 0.4 µm filter. PVA was spin-coated on the photoresist to form a 50 µm thick layer and baked at 100 °C for 2 h. The spin-coating was performed at low rotation velocity 20 rpm and acceleration 10 rpm s^{-1} for uniform thickness. After that, aluminum thin film was deposited and patterned on PVA layer. At last, the PVA substrate was delaminated from the glass slide by applying acetone to dissolve the photoresist. The described processing above is appropriate for small-area electronics. For large-area fabrication that requires inkjet printing for instance, the commercial product of PVA laminated on polyethylene terephthalate (PET) films (Aicello, SOLUBLON—30 µm thick PVA on 75 µm thick PET) performs better.

Thin Film Patterning: WTP technology required that the devices must be processed on the water-soluble substrate. Many approaches to solve this issue was already proposed.[35] In this study, a 150 nm thick aluminum film was deposited by thermal evaporation using a homemade equipment. Shadow mask or reactive ion etching (RIE) method was used to pattern the aluminum layer. After the classical lithographic process using S1818 photoresist, the aluminum pattern was etched in inductive coupled plasma (ICP)/RIE equipment with the experimental settings of 5 mTorr working pressure, 100 W plasma power, and chlorinated gas flow of 30 sccm.

Inkjet Printing of Polymeric Mesh: The inkjet printing was performed using CERADROP X-series printer. Inks were used without filtering. Epoxy-based ink (Su8-2000 series; MicroChem, Westborough, MA, USA) was printed using a 16-nozzle cartridge (Dimatix) with the experimental settings already reported.[44] The sample was baked at 95 °C for 5 min in an oven, followed by UV ($\lambda = 365$ nm) exposure, and baked again in an oven at 95 °C for 5 min.

Dipping and Transfer Steps: PVA film was placed on the water surface and dissolved. Then the object was dipped through the floating pattern into the water. After that, the object was withdrawn and dried. Van der Waals force allowed the pattern sticking to the 3D object. In this study, the adhesion forces were not quantified as they should be part of an independent study. However, after the object withdrawals, no delamination was ever observed, suggesting the robustness of the process. Moreover, the dipping velocity (2 mm·s^{-1}) was kept constant

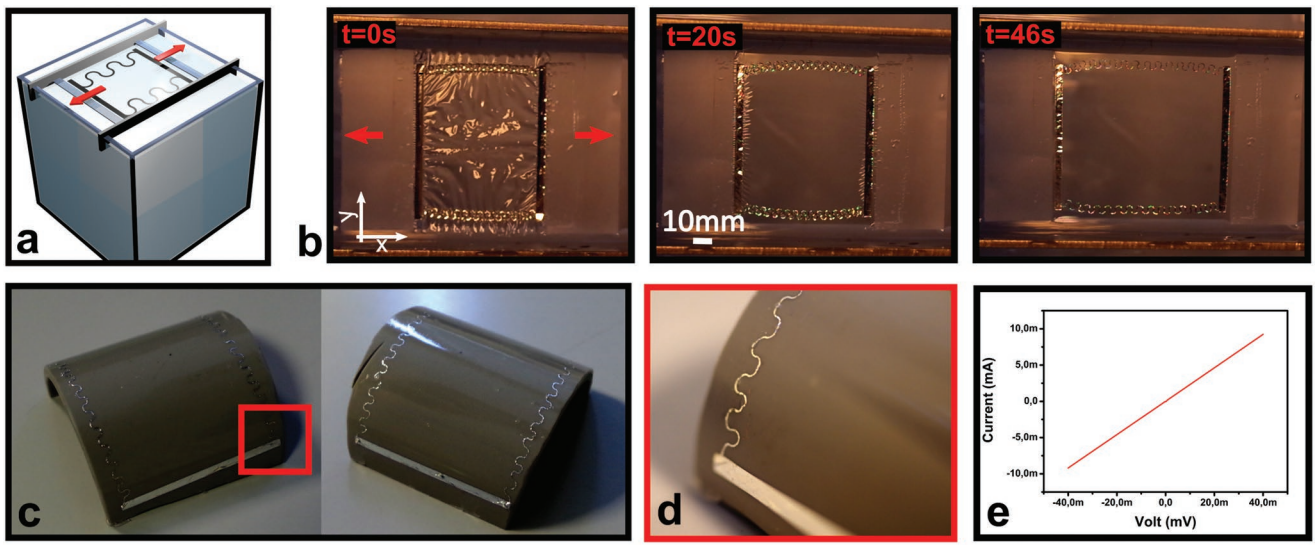

Figure 6. WTP process for serpentine-shaped interconnects. a) A 3D schematic of the setup with confining guides and mobile guides similar to Figure 4a. b) Snapshots of the uniaxial self-expansion of the serpentine ribbon. c) The serpentine ribbons transferred onto a hemicylindrical surface of 50 mm diameter. d) Zoomed in view. e) Electrical characteristics ($I = f(V)$) measured between the two straight ribbons interconnected by the serpentines after transfer.

for all the experiments. This velocity was fixed to minimize patterns distortion induced during the object dipping step as Zahng et al. did for hydrographic printing.[34] Furthermore, Zhang et al. developed an analytical model to calculate the pattern distortion for hydrographic printing a viscous ink layer.[34] However, such model cannot be directly applied in the study since the elastic metal structures in the study significantly increase the complexity of analytical model, which requires further work.

Rigid and Mobile Guides Setup: Rigid guides were made of stiff metal plates that were fixed on the side of the dip tank. The space between the plates was adjusted to fit the size of the PVA substrate. Mobile guides were made of commercial adhesive tapes that were well-aligned and attached on two parallel sides of the rectangular PVA substrate.

Serpentine Design: The thickness of aluminum thin film was 150 nm. The serpentine inner diameter and width were 600 and 200 µm, respectively. The undeformed end-to-end distance of a serpentine unit cell was 2000 µm.

Supporting Information

Supporting Information is available from the Wiley Online Library or from the author.

Acknowledgements

This work was supported by the European Union through the European Regional Development Fund (ERDF), and by the French region of Brittany (project: IMPRIM'), and by IETR (project: 3DELEC). N.L. acknowledges the support from US Air Force Office of Scientific Research (AFOSR) under Grant No. FA9550-15-1-0112. B.L.B. acknowledges the support from the EPSRC under Grant Next Generation Paper No. EP/P02579X/1.

Conflict of Interest

The authors declare no conflict of interest.

Keywords

conformable electronics, large-area electronics, stretchable electronics, surface tension, water transfer printing

Received: November 7, 2018
Revised: January 11, 2019
Published online:

[1] E. Y. Ma, S. Wagner, *Appl. Phys. Lett.* **1999**, *74*, 2661.
[2] M. L. Hammock, A. Chortos, B. C.-K. Tee, J. B.-H. Tok, Z. Bao, *Adv. Mater.* **2013**, *25*, 5997.
[3] T. Someya, S. Bauer, M. Kaltenbrunner, *MRS Bull.* **2017**, *42*, 124.
[4] D.-H. Kim, R. Ghaffari, N. Lu, J. A. Rogers, *Annu. Rev. Biomed. Eng.* **2012**, *14*, 113.
[5] W.-H. Yeo, Y.-S. Kim, J. Lee, A. Ameen, L. Shi, M. Li, S. Wang, R. Ma, S. H. Jin, Z. Kang, *Adv. Mater.* **2013**, *25*, 2773.
[6] S. H. Jeong, S. Zhang, K. Hjort, J. Hilborn, Z. Wu, *Adv. Mater.* **2016**, *28*, 5830.
[7] B. Xu, A. Akhtar, Y. Liu, H. Chen, W.-H. Yeo, S. I. Park, B. Boyce, H. Kim, J. Yu, H.-Y. Lai, S. Jung, Y. Zhou, J. Kim, S. Cho, Y. Huang, T. Bretl, J. A. Rogers, *Adv. Mater.* **2016**, *28*, 4462.
[8] R. Rogel, B. L. Borgne, T. Mohammed-Brahim, E. Jacques, M. Harnois, *Adv. Mater. Interfaces*1600946, **2017**, *4*.
[9] M. Stoppa, A. Chiolerio, *Sensors* **2014**, *14*, 11957.
[10] Y. J. Park, S.-K. Lee, M.-S. Kim, H. Kim, J.-H. Ahn, *ACS Nano* **2014**, *8*, 7655.
[11] M. Ha, S. Lee, H. Ko, *J. Mater. Chem. B* **2018**, *6*, 4043.
[12] P. Fattahi, G. Yang, G. Kim, M. R. Abidian, *Adv. Mater.* **2014**, *26*, 1846.
[13] Z. Fekete, A. Pongrácz, *Sens. Actuators, B* **2017**, *243*, 1214.
[14] S. P. Lacour, G. Courtine, J. Guck, *Nat. Rev. Mater.* **2016**, *1*, 16063.
[15] G. J. Lee, C. Choi, D.-H. Kim, Y. M. Song, *Adv. Funct. Mater.* **2018**, *28*, 1705202.
[16] H. Xu, L. Yin, C. Liu, X. Sheng, N. Zhao, *Adv. Mater.* **2018**, *30*, 1800156.
[17] T. Sekitani, H. Nakajima, H. Maeda, T. Fukushima, T. Aida, K. Hata, T. Someya, *Nat. Mater.* **2009**, *8*, 494.
[18] M. Vosgueritchian, J. B.-H. Tok, Z. Bao, *Nat. Photonics* **2013**, *7*, 769.
[19] J. H. Koo, D. C. Kim, H. J. Shim, T.-H. Kim, D.-H. Kim, *Adv. Funct. Mater.* **2018**, *28*, 1801834.
[20] M. Kaltenbrunner, M. S. White, E. D. Głowacki, T. Sekitani, T. Someya, N. S. Sariciftci, S. Bauer, *Nat. Commun.* **2012**, *3*, 770.
[21] M. Kaltenbrunner, T. Sekitani, J. Reeder, T. Yokota, K. Kuribara, T. Tokuhara, M. Drack, R. Schwödiauer, I. Graz, S. Bauer-Gogonea, S. Bauer, T. Someya, *Nature* **2013**, *499*, 458.
[22] G. A. Salvatore, N. Münzenrieder, T. Kinkeldei, L. Petti, C. Zysset, I. Strebel, L. Büthe, G. Tröster, *Nat. Commun.* **2014**, *5*, 2982.
[23] C. Choi, M. K. Choi, S. Liu, M. S. Kim, O. K. Park, C. Im, J. Kim, X. Qin, G. J. Lee, K. W. Cho, M. Kim, E. Joh, J. Lee, D. Son, S.-H. Kwon, N. L. Jeon, Y. M. Song, N. Lu, D.-H. Kim, *Nat. Commun.* **2017**, *8*, 1664.
[24] N. Lu, S. Yang, *Curr. Opin. Solid State Mater. Sci.* **2015**, *19*, 149.
[25] S. Yao, P. Swetha, Y. Zhu, *Adv. Healthcare Mater.* **2018**, *7*, 1700889.
[26] M. D. Dickey, *Adv. Mater.* **2017**, *29*, 1606425.
[27] A. Miyamoto, S. Lee, N. F. Cooray, S. Lee, M. Mori, N. Matsuhisa, H. Jin, L. Yoda, T. Yokota, A. Itoh, M. Sekino, H. Kawasaki, T. Ebihara, M. Amagai, T. Someya, *Nat. Nanotechnol.* **2017**, *12*, 907.
[28] N. Liu, A. Chortos, T. Lei, L. Jin, T. R. Kim, W.-G. Bae, C. Zhu, S. Wang, R. Pfattner, X. Chen, R. Sinclair, Z. Bao, *Sci. Adv.* **2017**, *3*, e1700159.
[29] S. Wang, J. Xu, W. Wang, G.-J. N. Wang, R. Rastak, F. Molina-Lopez, J. W. Chung, S. Niu, V. R. Feig, J. Lopez, T. Lei, S.-K. Kwon, Y. Kim, A. M. Foudeh, A. Ehrlich, A. Gasperini, Y. Yun, B. Murmann, J. B.-H. Tok, Z. Bao, *Nature* **2018**, *555*, 83.
[30] Y. Wang, C. Zhu, R. Pfattner, H. Yan, L. Jin, S. Chen, F. Molina-Lopez, F. Lissel, J. Liu, N. I. Rabiah, Z. Chen, J. W. Chung, C. Linder, M. F. Toney, B. Murmann, Z. Bao, *Sci. Adv.* **2017**, *3*, e1602076.
[31] J. Xu, S. Wang, G.-J. N. Wang, C. Zhu, S. Luo, L. Jin, X. Gu, S. Chen, V. R. Feig, J. W. To, S. Rondeau-Gagné, J. Park, B. C. Schroeder, C. Lu, J. Y. Oh, Y. Wang, Y.-H. Kim, H. Yan, R. Sinclair, D. Zhou, G. Xue, B. Murmann, C. Linder, W. Cai, J. B.-H. Tok, J. W. Chung, Z. Bao, *Science* **2017**, *355*, 59.
[32] H. Liu, Q. Li, S. Zhang, R. Yin, X. Liu, Y. He, K. Dai, C. Shan, J. Guo, C. Liu, C. Shen, X. Wang, N. Wang, Z. Wang, R. Wei, Z. Guo, *J. Mater. Chem. C* **2018**, *6*, 12121.
[33] J. J. Adams, E. B. Duoss, T. F. Malkowski, M. J. Motala, B. Y. Ahn, R. G. Nuzzo, J. T. Bernhard, J. A. Lewis, *Adv. Mater.* **2011**, *23*, 1335.
[34] Y. Zhang, C. Yin, C. Zheng, K. Zhou, *ACM Trans. Graphics (TOG)* **2015**, *34*, 131.
[35] B. Le Borgne, O. De Sagazan, S. Crand, E. Jacques, M. Harnois, *ACS Appl. Mater. Interfaces* **2017**, *9*, 29424.
[36] G. Saada, M. Layani, A. Chernevousky, S. Magdassi, *Adv. Mater. Technol.* **2017**, *2*, 1600289.
[37] L. W. Ng, X. Zhu, G. Hu, N. Macadam, D. Um, T.-C. Wu, F. L. Moal, C. G. Jones, T. Hasan, *ArXiv Prepr. ArXiv181101073* **2018**, 1.
[38] B. Le Borgne, E. Jacques, M. Harnois, *Micromachines* **2018**, *9*, 474.

[39] S. Cınar, R. Jamshidi, Y. Chen, N. Hashemi, R. Montazami, *J. Polym. Sci., Part B: Polym. Phys.* **2016**, *54*, 517.
[40] A. Bhattacharya, P. Ray, *J. Appl. Polym. Sci.* **2004**, *93*, 122.
[41] T. Widlund, S. Yang, Y.-Y. Hsu, N. Lu, *Int. J. Solids Struct.* **2014**, *51*, 4026.
[42] S. Yang, S. Qiao, N. Lu, *J. Appl. Mech.* **2017**, *84*, 021004.
[43] G. Mearini, R. Hoffman, *J. Electron. Mater.* **1993**, *22*, 623.
[44] S. J. Moon, M. Robin, K. Wenlin, M. Yann, B. S. Bae, T. Mohammed-Brahim, E. Jacques, M. Harnois, *Flexible Printed Electron.* **2017**, *2*, 035008.